Breaking the Speed Limits of Phase-Change Memory

D. Loke *et al.*

Science **336**, 1566 (2012);
DOI: 10.1126/science.1221561

References and Notes

1. M. Wuttig, N. Yamada, *Nat. Mater.* **6**, 824 (2007).
2. S. Raoux, *Annu. Rev. Mater. Res.* **39**, 25 (2009).
3. Y. Jung, S. W. Nam, R. Agarwal, *Nano Lett.* **11**, 1364 (2011).
4. B. J. Kooi, W. M. G. Groot, J. T. M. De Hosson, *J. Appl. Phys.* **95**, 924 (2004).
5. P. Fons *et al.*, *Phys. Rev. B* **82**, 041203(R) (2010).
6. A. V. Kolobov, M. Krbal, P. Fons, J. Tominaga, T. Uruga, *Nat. Chem.* **3**, 311 (2011).
7. D. R. Strachan *et al.*, *Phys. Rev. Lett.* **100**, 056805 (2008).
8. S. H. Lee, Y. Jung, R. Agarwal, *Nat. Nanotechnol.* **2**, 626 (2007).
9. S. W. Nam *et al.*, *Electrochem. Solid-State Lett.* **12**, H155 (2009).
10. T. Y. Yang, I. M. Park, B. J. Kim, Y. C. Joo, *Appl. Phys. Lett.* **95**, 032104 (2009).
11. M. H. Lee *et al.*, *IEEE International Electron Devices Meeting (IEDM)*, 28.6.1. (2010).
12. G. Schoeck, W. A. Tiller, *Philos. Mag.* **5**, 43 (1960).
13. H. Kimura, R. Maddin, D. Kuhlmannwilsdorf, *Acta Metall.* **7**, 145 (1959).
14. H. Zheng *et al.*, *Nat. Commun.* **1**, 144 (2010).
15. Z. W. Shan, R. K. Mishra, S. A. Syed Asif, O. L. Warren, A. M. Minor, *Nat. Mater.* **7**, 115 (2008).
16. S. H. Oh, M. Legros, D. Kiener, G. Dehm, *Nat. Mater.* **8**, 95 (2009).
17. Q. Yu *et al.*, *Nature* **463**, 335 (2010).
18. T. Zhu, J. Li, A. Samanta, A. Leach, K. Gall, *Phys. Rev. Lett.* **100**, 025502 (2008).
19. M. Mitra, Y. Jung, D. S. Gianola, R. Agarwal, *Appl. Phys. Lett.* **96**, 222111 (2010).
20. R. H. Telling, M. I. Heggie, *Philos. Mag. Lett.* **83**, 411 (2003).
21. A. V. Kolobov *et al.*, *Nat. Mater.* **3**, 703 (2004).
22. Z. M. Sun, J. Zhou, R. Ahuja, *Phys. Rev. Lett.* **96**, 055507 (2006).
23. S. Ogata, J. Li, S. Yip, *Phys. Rev. B* **71**, 224102 (2005).
24. E. Kaxiras, M. S. Duesbery, *Phys. Rev. Lett.* **70**, 3752 (1993).
25. D. Hull, D. J. Bacon, *Introduction to Dislocations* (Butterworth-Heinemann, Oxford, ed. 4, 2001).
26. K. Nagel, *Phys. Rev. E Stat. Phys. Plasmas Fluids Relat. Interdiscip. Topics* **53**, 4655 (1996).
27. D. Helbing, *Rev. Mod. Phys.* **73**, 1067 (2001).
28. D. Wolf, P. R. Okamoto, S. Yip, J. F. Lutsko, M. Kluge, *J. Mater. Res.* **5**, 286 (1990).
29. J. Y. Huang, H. Yasuda, H. Mori, *Philos. Mag. Lett.* **79**, 305 (1999).
30. J. Y. Huang *et al.*, *Science* **330**, 1515 (2010).
31. J. Y. Huang, Y. T. Zhu, X. Z. Liao, R. Z. Valiev, *Philos. Mag. Lett.* **84**, 183 (2004).
32. Y. Mishin, M. Asta, J. Li, *Acta Mater.* **58**, 1117 (2010).
33. A. V. Kolobov *et al.*, *Phys. Rev. Lett.* **97**, 035701 (2006).

Acknowledgments: This work was supported by the Office of Naval Research (grant N000140910116), Materials Structures and Devices Center at the Massachusetts Institute of Technology, NSF (DMR-0706381 and DMR-1002164), and Penn-Materials Research Science and Engineering Center (DMR05-20020 and DMR11-20901). Y.C.L., L.Q., and J.L. acknowledge the support of NSF DMR-1008104 and DMR-1120901, and Air Force Office of Scientific Research FA9550-08-1-0325. Y.L. and A.T.C.J. acknowledge the support of the Nano/Bio Interface Center through NSF Nanoscale Science and Engineering Center DMR08-32802. Electron microscopy experiments were performed at the Penn Regional Nanotechnology Facility at the University of Pennsylvania. S.-W.N. thanks D. Strachan for useful discussions on in situ TEM experiments. The data described in the paper are archived by the Agarwal group at the University of Pennsylvania.

Supplementary Materials

www.sciencemag.org/cgi/content/full/336/6088/1561/DC1
Materials and Methods
Figs. S1 to S15
References
Movies S1 to S3

6 February 2012; accepted 18 May 2012
10.1126/science.1220119

Breaking the Speed Limits of Phase-Change Memory

D. Loke,[1,2,3]* T. H. Lee,[2]* W. J. Wang,[1] L. P. Shi,[1]† R. Zhao,[1] Y. C. Yeo,[4] T. C. Chong,[5] S. R. Elliott[2]†

Phase-change random-access memory (PCRAM) is one of the leading candidates for next-generation data-storage devices, but the trade-off between crystallization (writing) speed and amorphous-phase stability (data retention) presents a key challenge. We control the crystallization kinetics of a phase-change material by applying a constant low voltage via prestructural ordering (incubation) effects. A crystallization speed of 500 picoseconds was achieved, as well as high-speed reversible switching using 500-picosecond pulses. Ab initio molecular dynamics simulations reveal the phase-change kinetics in PCRAM devices and the structural origin of the incubation-assisted increase in crystallization speed. This paves the way for achieving a broadly applicable memory device, capable of nonvolatile operations beyond gigahertz data-transfer rates.

Phase-change random-access memory (PCRAM) represents one of the best candidates for a so-called "universal memory" due to its nonvolatile nature, high scalability, low power consumption, high read/write speeds, and long read/write endurance (*1*–*4*). PCRAM operations, based on the reversible switching of phase-change (PC) materials between amorphous and crystalline states (*5*, *6*), are generally fast: on the order of nanosecond time scales (*7*–*9*). However, the crystallization speed is much slower than the amorphization speed, which limits the overall writing speed of PCRAMs. Despite efforts (*10*–*16*) to increase the crystallization speed, it has been difficult to achieve a speed faster than 1 ns. A difficulty arises from the contradictory nature of increasing the crystallization speed while extending the stability of PC materials for long-term data retention (*17*). This has restricted the selection of PC materials in the commercial development of PCRAMs, typically emphasizing high stability at the expense of crystallization speeds.

According to classical nucleation theory, the nucleation of small crystallites and their subsequent growth are the two main distinct processes in crystallization (*18*–*20*). The nucleation rate is faster at lower temperatures, followed by rapid growth at higher temperatures (*21*). We show that by stimulating and altering these processes, we are able to control the speed of crystallization by electrical means. Our approach is based on the idea of providing a weak electric field to induce thermal prestructural ordering (incubation of ordered clusters in the amorphous matrix) via Joule heating, which enables faster nucleation and growth upon a subsequent stronger electrical pulse, while maintaining the high stability of the amorphous phase by controlling the cluster-size distribution (Fig. 1). This thermal-incubation model is very different from the model of Karpov *et al.* (*22*), which assumes a direct electric-field–induced modification of the crystal-nucleation barriers in $Ge_2Sb_2Te_5$ (GST).

We experimentally fabricated porelike structured PCRAM cells (with GST as the PC material) and used these cells to study the incubation effects on the crystallization speeds (Fig. 1D) (*23*). To study the ultrafast switching effects, a weak electric field (equivalent to ~0.3 V), for tailoring the crystallization kinetics (hereafter referred to as the incubation field), was employed to achieve optimal switching properties without activating spontaneous crystallization (fig. S2). We employed subsequent electrical pulses (varying in length from several hundred picoseconds to several tens of nanoseconds) to switch the cells, and we used the full width at half maximum (FWHM) values of the pulses to characterize the switching speeds of the cells (fig. S3). The duration of a pulse experienced in the cell was confirmed to be the same as that measured before the pulse enters the cell (fig. S4).

We found that the incubation field, even with the small amount of thermal energy it delivers, can substantially promote the nucleation and growth of PC materials. Nucleation and growth times can be characterized by the minimum electrical pulse width needed to switch the cell from the amorphous state to the crystalline state (*24*), also known as the "set" process. When the incubation field is applied to a cell (Fig. 2A), much faster nucleation and growth are observed, as manifested by the substantial decrease in pulse width (by ~5 ns). For the fastest nucleation and growth, we found the shortest pulse to be 500 ps. This is approximately one order of magnitude

[1]Data Storage Institute, Agency for Science, Technology and Research (A*STAR), 5 Engineering Drive 1, Singapore 117608. [2]Department of Chemistry, University of Cambridge, Lensfield Road, Cambridge CB2 1EW, UK. [3]National University of Singapore (NUS) Graduate School for Integrative Sciences and Engineering, 28 Medical Drive, Singapore 117456. [4]Department of Electrical and Computer Engineering, National University of Singapore, 4 Engineering Drive 3, Singapore 117576. [5]Singapore University of Technology and Design, 20 Dover Drive, Singapore 138682.

*These authors contributed equally to this work.
†To whom correspondence should be addressed. E-mail: shi_luping@dsi.a-star.edu.sg (L.P.S.); sre1@cam.ac.uk (S.R.E.)

faster than the fastest switching speeds previously achieved in GST/GeTe cells with similar sizes under full recrystallization conditions and with the use of the voltage-peak FWHM as a measure of the pulse duration (*7*, *8*).

Fast crystallization speeds facilitated by an incubation field can be achieved without affecting the amorphization of PC materials (the "reset" process). The reset process involves the melting of the material at high temperatures, followed by the rapid quenching of the material to the amorphous state. The reset process under an incubation field is also very fast. Amorphization speeds as fast as 500 ps were also achieved (fig. S5). More importantly, upon applying the incubation field, we discovered that a cell can be switched reversibly and stably with set and reset pulses both equal to 500 ps for 10^4 cycles (Fig. 2B). We also observed that both the resistance of the amorphous state and the reset/set resistance ratio are relatively constant during the cycling experiment. These results show that both fast speed and stability of the amorphous phase can be achieved simultaneously.

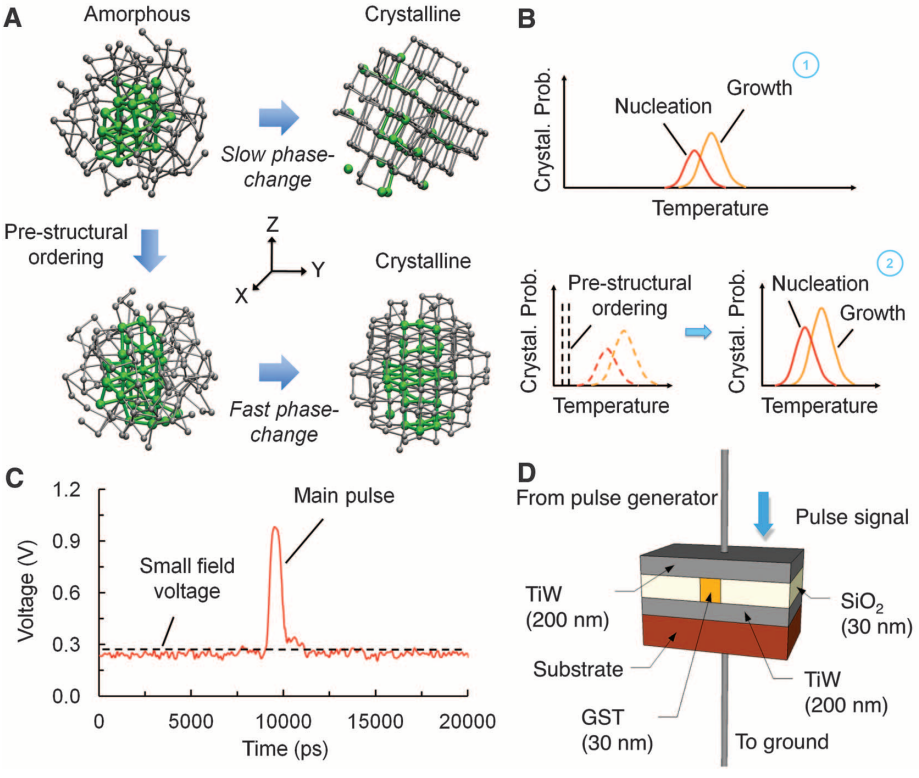

Fig. 1. Prestructural ordering effects on the crystallization of PC materials. (**A**) Model configurations demonstrating the atomic rearrangements during the phase transition, with and without prestructural ordering. (**B**) Schematics of the crystallization probability as a function of temperature for PC materials. The nucleation and growth processes are accelerated when there is prestructural ordering (from method 1 to 2). (**C**) Waveform of a small-field incubation voltage and main pulse applied to set the PCRAM. A small voltage is first applied to initiate prestructural ordering, followed by a main pulse to induce crystal nucleation and growth of the PC material. (**D**) Schematic of the PCRAM structure with the pulse signal delivered to heat and crystallize the PC material (GST).

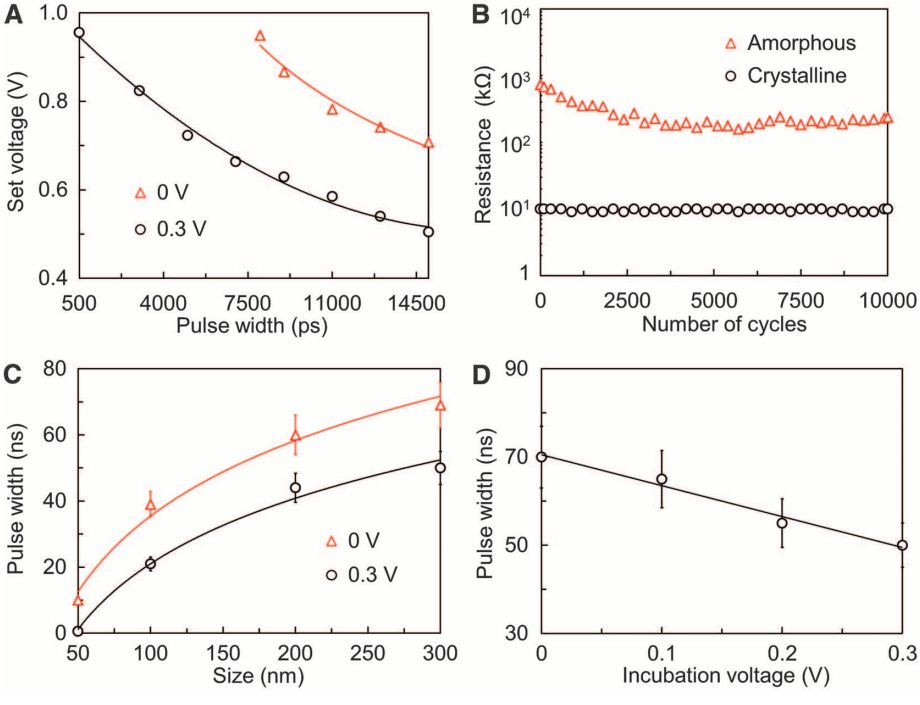

Fig. 2. PCRAM switching properties. (**A**) Dependence of minimum voltage on the pulse width achieved by a PCRAM cell (50 nm) under incubation-field conditions (0.3 V). The fastest speed achieved was 500 ps. (**B**) Reversible switching of PCRAM. Fast and stable switching with 500-ps pulses for both set (1 V) and reset (6.5 V) processes is observed for 10^4 cycles. (**C**) Size-dependent switching speed of PCRAM. Shorter pulse widths are achieved when the cell size is decreased for a fixed applied-voltage pulse (1 V). The pulse width decreases additionally when the incubation field (0.3 V) is applied, further improving the speed of PCRAM. (**D**) Minimum pulse width versus incubation field (voltage) for a PCRAM cell (300 nm). The pulse width reduces as the incubation field increases, revealing the incubation-dependent crystallization speed of PC materials.

Even faster crystallization is observed when the incubation field is applied to cells with smaller feature sizes. In general, PC materials are divided into two groups, depending on the crystallization mechanism. For nucleation-dominated crystallization, a large number of crystalline nuclei form in the amorphous region. For growth-dominated crystallization, the transformation of the amorphous region is directed by the growth of the crystalline phase from the crystalline rim surrounding the amorphous region/interface between the PC material and dielectric sidewalls in optical and electrical PC devices (*8*, *25*, *26*). Growth-dominated crystallization can be characterized by the strong dependence of crystallization time on the size of the amorphous/active region (in this case, cell size). This growth-dominance effect can be seen in Fig. 2C where, under no incubation field, the pulse width for set reduces from 70 to 10 ns as the cell size decreases from 300 to 50 nm. A very different effect is observed when an incubation field is applied. We found that the pulse width decreases even more substantially as the cell size decreases (by 28% at 300 nm and by 95% at 50 nm), suggesting a much faster nucleation and growth induced by a combination of size and incubation effects.

One of the key results of our study is the ability to control the crystallization speed (nucleation and growth time) by varying the intensity of the incubation field. This implies that nucleation and growth can be further accelerated via stronger incubation fields. Figure 2D shows the pulse width needed to set a cell (300 nm) at different incubation fields. We observed that the pulse width decreases from 70 to 50 ns as the incubation field increases (0 to 0.3 V), revealing the dependence of the crystallization speed of PC materials on the intensity of the incubation field. Previous works on GST (*27*) and Ag-In-Sb-Te (*28*, *29*), using optical (laser pump-probe) stimulation and direct thermal-annealing treatment, have also shown that the crystal-nucleation rate can be manipulated. However, the crystallization times achieved in those studies were on the order of only several tens of nanoseconds to a few microseconds.

The microscopic origin of the ultrafast crystallization resulting from the application of an incubation field was investigated by performing ab initio molecular dynamics (AIMD) simulations for 180-atom models of GST (*23*). To simulate the crystallization process on the application of incubation fields and/or electrical pulses, two temperatures of 420 and 600 K were applied to the GST models to mimic the respective annealing/Joule-heating processes (hereafter, annealing at 420 K is referred to as "preannealing") (fig. S6). The detailed procedures for simulating the amorphous-to-crystal phase transition are described in fig. S7. For a more complete (statistical) analysis, we studied three amorphous (a-) models (models 1 to 3), which were obtained by independently quenching different configurations of liquid GST. The basic structural units of crystalline GST (that is, of the metastable distorted rock salt structure)—such as fourfold rings, planes, and cubes—were used to characterize the local structural order (or the crystallization process during annealing) (*23*).

To investigate the effects of applying an incubation field on the crystallization behavior, one of the a- models (*3*) was preannealed at 420 K for 270 ps and subsequently annealed at 600 K. For comparison, the same model was also annealed at only 600 K. In both cases, we examined the crystallization process by studying the evolution of the number of cubes; the onset time (t_o) of crystallization is defined here as the starting point of the increase of the stable cube cluster, whereas the end of crystallization is the point at which no further growth in the number of cubes is observed.

We observed much faster crystallization in the preannealed model, as shown in Fig. 3A. There is a large decrease in t_o for the preannealed model (~80 ps) compared with the model that was not preannealed (~350 ps). We also observed a similar shortening in t_o for another model that

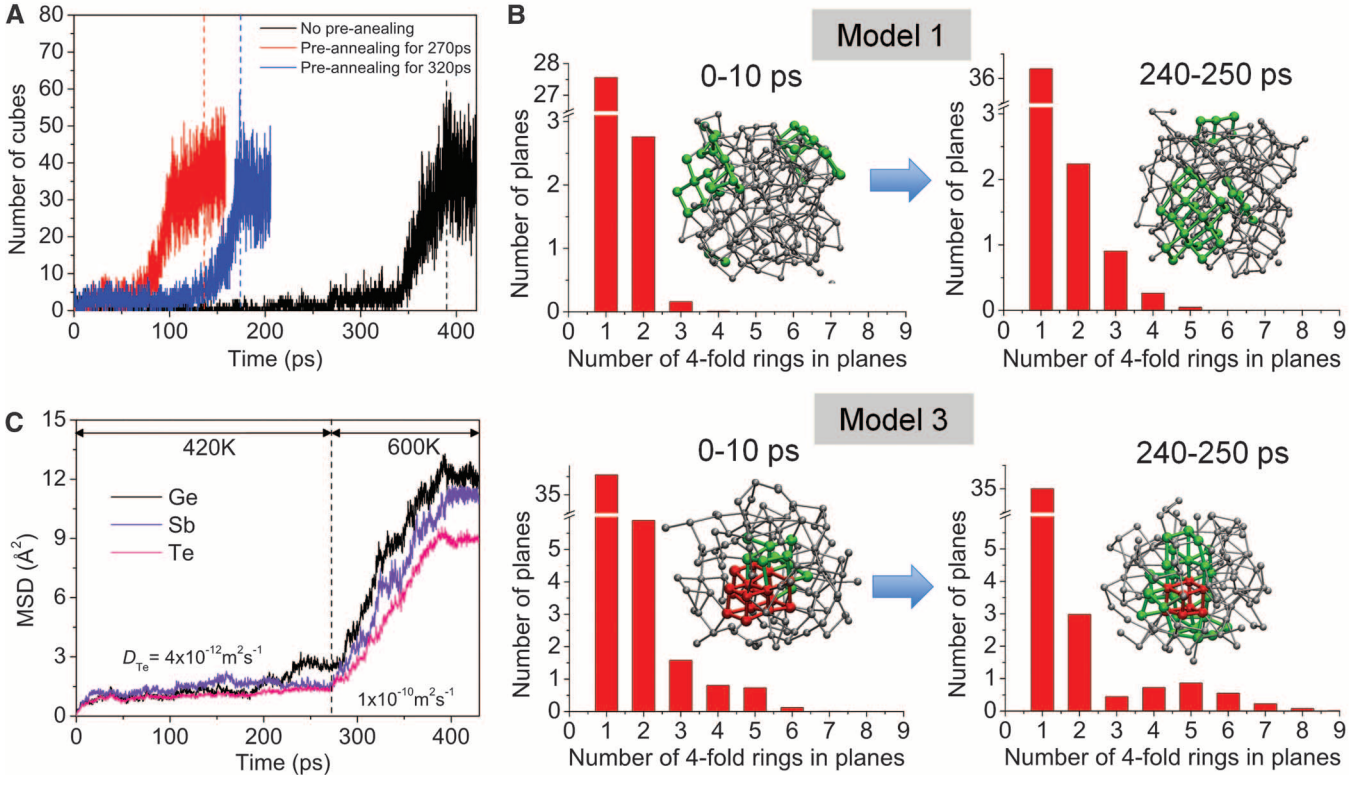

Fig. 3. AIMD simulations. (**A**) Variation of the number of cubes during annealing at 600 K with different preannealing times. (**B**) Population of fourfold rings and planes, composed of different numbers of fourfold rings, in model 1 before and after preannealing. The number of planes was averaged over the time interval denoted above each panel. A similar change in the distribution of the number of planes is seen in model 3. Green atoms are in planes; red atoms are in cubes. (**C**) Mean-squared displacement data for each type of atom during two successive annealing steps at 420 and 600 K (model 3). Diffusion coefficients for Te atoms (D_{Te}), calculated at each annealing temperature, are shown as an example.

was preannealed for longer times. The corresponding changes in the atomic structures for these two different annealing routes are shown in Fig. 1A, which explains the origin of the faster crystallization. Before t_o, there were substantial thermal fluctuations upon annealing at 600 K that resulted in the disruption of the initial cluster in the model that was not preannealed. After a period of repeated generation and annihilation of transient clusters (incubation time), a stable cluster (with a different orientation from the initial one) formed and grew to crystallize. This is not the case for the preannealed models; the initial ordered structure (further grown during preannealing) maintains its shape and grows along its original symmetry axis throughout the crystallization. Thus, the shortening in t_o for the preannealed models is associated with shorter incubation times for nucleation and growth, which is triggered by the structural ordering during preannealing.

We found that the predominant structural-ordering mechanism is the formation and growth of clusters of planes of fourfold rings (i.e., a structural feature of the rocksalt structure of the crystalline phase of GST), as shown in Fig. 3B. An overall medium-range ordering in the amorphous phase (in terms of the bond angles and atomic distances with the second-nearest neighbors) is also revealed (fig. S8).

This prestructural ordering is stable in nature. Figure 3C shows the mean-squared displacements of atoms during the two-step annealing process. The diffusion coefficient at 420 K is estimated to be about two orders of magnitude smaller than at 600 K. Accordingly, the structural ordering in a- GST at 420 K was found to be diffusionless; the formation and/or growth of a cluster of planes occurs mostly via cooperative (bond-rotational) movements (over much less than interatomic distances) of a few relevant atoms, in direct contrast to the structural ordering at 600 K induced by bond-breaking diffusional processes (fig. S10). This difference in behavior is most likely due to insufficient thermal energy available at 420 K to overcome the energy barrier for diffusion. Consequently, the growth speed and the size of clusters at this low temperature should be kinetically limited, in spite of the driving force for nucleation (that is, free-energy difference) being greater than at higher temperatures (*30*).

Important observations from our simulations are as follows: (i) In general, annealing at low temperatures (at least at 420 K, which is much lower than the peak crystallization temperature) leads to medium-range structural ordering in a- GST, including the formation (and growth) of clusters (prestructural ordering). (ii) Prestructural ordering can induce faster crystallization via shorter incubation times for the nucleation upon subsequent annealing at higher temperatures.

The origin of the faster crystallization under the influence of the incubation field can be similarly understood with the help of the concept of a cluster-size distribution, the basis of the kinetic model of nucleation (*31*, *32*). Specifically, applying an incubation field induces a temperature increase (~100 K) by Joule heating. This elevated temperature is not high enough to activate spontaneous nucleation and growth; it simply leads to an overall structural ordering with the development of clusters in the amorphous matrix, which is important for the amorphous stability. Naturally, a new cluster-size distribution results at this temperature, where the population of larger clusters (mostly smaller than the critical nucleus size) becomes more abundant. A greater population of larger clusters (as well as overall medium-range ordering) then enhances the probability of successful nucleation (via shorter incubation times required for nucleation) and of subsequent growth, when an electrical pulse is applied, the energy of which is high enough to activate diffusion-induced structural ordering. Thus, the electrical controllability of the crystallization speed (as in Fig. 2D) is closely associated with the effect of temperature on the cluster-size distribution that determines the nucleation probability. On the atomic scale, such structural ordering, even at a low temperature, seems to be a general feature of PC materials, being enabled by the intrinsic electronic configurations of the constituent atoms, facilitating pure *p*-bonding (*33*).

The experimental and simulation findings show that ultrafast crystallization can be achieved by applying an incubation electrical field. The additional energy needed to apply the incubation field is much smaller than that for crystallization, as the applied incubation voltage is much less than the typical threshold-switching voltage (0.5 to 1 V). Furthermore, the incubation field can be applied after a reset process for a minimum time (fig. S11). This reduces the extra energy needed, in contrast to applying the incubation field consistently, while waiting for the set process in real device operations. To further reduce the energy required, PCRAM can also be operated from a lower resistance level (fig. S12).

In addition to showing rapid crystallization speeds, we also show the endurance of memory cells operating at such high speeds. This indicates that our approach is feasible for device applications.

These rapid crystallization times, as well as high amorphous-state stability, are achieved through an electrically induced incubation process in PCRAM devices that alters the crystallization kinetics of the a- GST. In principle, this method is applicable to all types of PC materials and memory-device structures, so that an appropriate combination of programming schemes and PC materials opens opportunities for optimizing PCRAM device performance.

References and Notes

1. S. Lai, T. Lowrey, in *IEDM Tech. Digest* (IEEE International Electron Devices Meeting, Washington, DC, 2 to 5 December 2001), pp. 36.5.1–36.5.4; 10.1109/IEDM.2001.979636.
2. A. Pirovano *et al.*, in *IEDM Tech. Digest* (IEEE International Electron Devices Meeting, Washington, DC, 8 to 10 December 2003), pp. 29.6.1–29.6.4; 10.1109/IEDM.2003.1269376.
3. M. Wuttig, *Nat. Mater.* **4**, 265 (2005).
4. H.-S. P. Wong *et al.*, *Proc. IEEE* **98**, 2201 (2010).
5. S. R. Ovshinsky, *Phys. Rev. Lett.* **21**, 1450 (1968).
6. D. Adler, H. K. Henisch, N. F. Mott, *Rev. Mod. Phys.* **50**, 209 (1978).
7. W. J. Wang *et al.*, *Appl. Phys. Lett.* **93**, 043121 (2008).
8. G. Bruns *et al.*, *Appl. Phys. Lett.* **95**, 043108 (2009).
9. D. Loke *et al.*, *Nanotechnology* **22**, 254019 (2011).
10. M. H. R. Lankhorst, B. W. S. M. M. Ketelaars, R. A. M. Wolters, *Nat. Mater.* **4**, 347 (2005).
11. S.-H. Lee, Y. Jung, R. Agarwal, *Nat. Nanotechnol.* **2**, 626 (2007).
12. F. Xiong, A. D. Liao, D. Estrada, E. Pop, *Science* **332**, 568 (2011).
13. T. C. Chong *et al.*, *Appl. Phys. Lett.* **88**, 122114 (2006).
14. Y. H. Ha *et al.*, in *Symp. VLSI Tech.* (IEEE Symposium on VLSI Technology, Kyoto, Japan, 10 to 12 June 2003), pp. 175–176; 10.1109/VLSIT.2003.1221142.
15. F. Pellizzer *et al.*, in *Symp. VLSI Tech.* (IEEE Symposium on VLSI Technology, Honolulu, HI, 15 to 17 June 2004), pp. 18–19; 10.1109/VLSIT.2004.1345368.
16. H. Horii *et al.*, in *Symp. VLSI Tech.* (IEEE Symposium on VLSI Technology, Kyoto, Japan, 10 to 12 June 2003), pp. 177–178; 10.1109/VLSIT.2003.1221143.
17. N. Yamada, E. Ohno, K. Nishiuchi, N. Akahira, M. Takao, *J. Appl. Phys.* **69**, 2849 (1991).
18. J. H. Coombs, A. P. J. M. Jongenelis, W. van Es-Spiekman, B. A. J. Jacobs, *J. Appl. Phys.* **78**, 4918 (1995).
19. T. H. Jeong, M. R. Kim, H. Seo, S. J. Kim, S. Y. Kim, *J. Appl. Phys.* **86**, 774 (1999).
20. S. Raoux, J. L. Jordan-Sweet, A. J. Kellock, *J. Appl. Phys.* **103**, 114310 (2008).
21. J. Orava, A. L. Greer, B. Gholipour, D. W. Hewak, C. E. Smith, *Nat. Mater.* **11**, 279 (2012).
22. V. G. Karpov, Y. A. Kryukov, S. D. Savransky, I. V. Karpov, *Appl. Phys. Lett.* **90**, 123504 (2007).
23. Materials and methods are available as supplementary materials on *Science* Online.
24. E. G. Yeo *et al.*, *Appl. Phys. Lett.* **94**, 243504 (2009).
25. G.-F. Zhou, *Mater. Sci. Eng. A* **304–306**, 73 (2001).
26. N. Ohshima, *J. Appl. Phys.* **79**, 8357 (1996).
27. P. K. Khulbe, E. M. Wright, M. Mansuripur, *J. Appl. Phys.* **88**, 3926 (2000).
28. B.-S. Lee *et al.*, *Science* **326**, 980 (2009).
29. Y. Wang *et al.*, *Proc. SPIE* **7517**, 75170S (2009).
30. J. W. Christian, *The Theory of Transformations in Metals and Alloys: Part I Equilibrium and General Kinetic Theory* (Pergamon, Oxford, ed. 2, 1975).
31. M. Volmer, A. Weber, *Z. Phys. Chem.* **119**, 277 (1926).
32. D. Turnbull, J. C. Fisher, *J. Chem. Phys.* **17**, 71 (1949).
33. T. H. Lee, S. R. Elliott, *Phys. Rev. Lett.* **107**, 145702 (2011).

Acknowledgments: We acknowledge support by the Advanced Memory Research Program of A*STAR, the Nonvolatile Memory Research Program of Data Storage Institute (Singapore), and the Engineering and Physical Sciences Research Council (UK). The experiments were carried out in the Data Storage Institute, A*STAR, and the AIMD simulations were performed using the Cambridge High-Performance Computing Facility. D.L. thanks the NUS Graduate School for Integrative Sciences and Engineering for scholarship support.

Supplementary Materials

www.sciencemag.org/cgi/content/full/336/6088/1566/DC1
Materials and Methods
Figs. S1 to S12
References (*34*–*44*)

6 March 2012; accepted 10 April 2012
10.1126/science.1221561